PERGAMON

Available online at www.sciencedirect.com

SCIENCE DIRECT®

Engineering Fracture Mechanics 70 (2003) 2149–2162

Engineering Fracture Mechanics

www.elsevier.com/locate/engfracmech

Failure prediction analysis for polyethylene flawed pipes

Celina Bernal *, Hugo López Montenegro, Patricia Frontini

Institute of Materials Science and Technology (INTEMA), University of Mar del Plata and National Research Council (CONICET), J.B. Justo 4302, B7608FDQ Mar del Plata, Argentina

Received 12 June 2002; received in revised form 17 October 2002; accepted 19 October 2002

Abstract

Through this paper limit load analysis and the EPRI/GE procedure were applied to predict instability conditions for medium density polyethylene flawed pipes. Predicted values for internally pressurized cylinders with axial cracks and cylinders with circumferential cracks under remote tension were compared to experimental results obtained from tests conducted on full scale structures. For the pipes under internal pressure, both schemes led to critical pressure values in agreement with actual burst pressures, despite plastic collapse having been observed in the failure of these structures. For the pipes with circumferential internal cracks subjected to remote tension, the predicted loads from the EPRI procedure do not agree with experimental values whereas limit load predictions are quite satisfactory. On the other hand, for the circumferentially externally cracked pipes both predictions reasonable agree with experimental data.

Keywords: *J*-integral; Fracture mechanics; Failure assessment; Polyethylene pipes

1. Introduction

Over the recent years, the application of polyethylenes as structural materials has greatly increased, hence the study of their fracture behavior has received significant attention by the polymer community. Many works have been reported in literature concerning the failure behavior of pipe grade polyethylenes as well as on testing methodologies [1–11]. The integrity assessment of defective structures is particularly important in those cases, such as in polyethylene water and gas distribution pipelines, where the consequences of structural failures may be catastrophic.

A commonly used scheme to estimate maximum load in a structure is the limit load analysis. Its applicability is restricted to fixed dimensions structures that develop a reasonable amount of plasticity before maximum load. Structures containing crack-like defects may undergo ductile crack extension and therefore

* Corresponding author. Tel.: +54-223-4816600; fax: +54-223-4810046.
E-mail address: crbernal@fi.mdp.edu.ar (C. Bernal).

0013-7944/03/$ - see front matter © 2002 Elsevier Ltd. All rights reserved.
doi:10.1016/S0013-7944(02)00239-4

Nomenclature

J	J-integral
A	area under the load–displacement record
a	crack length
B	specimen thickness
W	specimen width
F	load
P	pressure
v	displacement
σ	stress
σ_0	yield stress
ε	deformation
α, ε_0 and n	power-law stress–strain approximation parameters
h	functions tabulated in the EPRI/GE Handbook
L_1	characteristic length of the structure
F_0	normalizing load
P_0	normalizing pressure
Δa	crack extension
c	uncracked ligament
E	Young's modulus
v	Poisson's ratio
E'	$E/(1-v^2)$
a_e	effective crack length
K	stress intensity factor in Mode I
S	support span
F_1 and h_1	functions tabulated in the EPRI/GE Handbook
R_i	pipe inner radius
R_o	pipe outer radius
R_c	radial distance from the centerline to the crack tip
P_{atm}	atmospheric pressure
σ^∞	remote uniform tensile stress

change their dimensions. In such cases a limit load solution alone is not enough and another criterion based on the material fracture toughness has to be used in order to determine crack length during loading [12].

On the other hand, the EPRI/GE estimation technique described in the General Electric Fracture Handbook [13] offers a simple and attractive approach to design and safety analysis of defective structures. Although this scheme is widely adopted for metals and in general, the agreement between the predicted and measured values is very good, confidence in its use for polymers is still controversial due to the scarce number of experimental data available.

The purpose of this paper was to analyze the capability of the EPRI and the limit load approaches to predict instability conditions in the case of a medium density polyethylene pressurized cylinder with an internal axial crack and a medium density polyethylene cylinder with a circumferential crack under remote tension. The procedure proposed in the EPRI/GE Handbook as well as the limit load analysis were applied and the results obtained from these schemes were compared to experimental results obtained from tests conducted on full scale structures.

2. Methodologies

2.1. Limit load analysis

When a reasonable amount of plasticity occurs before maximum load [12], critical loads or pressures can be calculated from the yield stress of the material and the effective cross-section of the samples for different crack lengths by using the appropriate formulae and by assuming that the main effect of the crack is to reduce the net cross-section of the structure [14].

For the case of an internally pressurized cylinder with an axial crack, the critical pressure P_c was calculated as follows by assuming the pipe as a thin-walled pipe [15]:

$$P_c = P_{atm} + \sigma_0 c/R_i \tag{1}$$

where P_{atm} is the atmospheric pressure, σ_0 is the yield stress of the material, c is the uncracked ligament and R_i is the pipe inner radius.

For a circumferentially internally cracked cylinder under remote tension, the critical load F_c was determined from

$$F_c = \sigma_0 \pi (R_o^2 - R_c^2) \tag{2}$$

whereas for a circumferentially externally cracked cylinder under remote tension, the critical load F_c was calculated as

$$F_c = \sigma_0 \pi (R_c^2 - R_i^2) \tag{3}$$

where R_o and R_i are the pipe outer and inner radii respectively and R_c is the radial distance from the centerline to the crack tip.

2.2. EPRI/GE prediction

The GE Handbook [13] contains tabulated functions which are normalized finite-element solutions for power-law plastic materials which can be used as schemes for the integrity assessment of defective structures.

Solutions have the following general form. The plastic strain is related to stress by a simple power-law:

$$\varepsilon/\varepsilon_0 = \alpha(\sigma/\sigma_0)^n \tag{4}$$

where α, σ_0, ε_0 and n are material constants. For any particular geometry the corresponding elastic–plastic values of J may be expressed in terms of dimensionless f_1 and h_1 functions as:

$$J = f_1(a_e; R_i/R_o)\frac{Q^2}{E'} + \alpha\varepsilon_0\sigma_0 L_1 h_1(a/b, n; R_i/R_o)(Q/Q_0)^{n+1} \tag{5}$$

where a is the crack length, a_e is the effective crack length in plane strain, E' is $E/(1-\nu^2)$ for plane strain, B is the section thickness, L_1 is a length characteristic of the structures, Q is the applied stress or load and Q_0 is a normalizing stress or load. The use of a simple power-law in Eq. (4) allows the dependence of J on stress or load to be included by the normalization in Eq. (5).

The EPRI/GE procedure allows the instability condition determination by comparing the crack driving force diagram with the material resistance to crack growth curve. A J-integral crack driving force diagram was generated in the range of values for crack length and applied loads or pressures obtained in the experiments. From the material stress–strain power-law constants and the respective elastic–plastic solutions J versus a curves having Q as the parameter were simply constructed from Eq. (5). Then, the instability point was determined from the constant load or pressure line which was tangent to the J–R curve.

Specific equations for the two geometries studied here are reported in the EPRI Handbook [16] and were used in this paper to predict failure of cracked pipes structures. These equations are transcribed in Appendix A.

J-resistance curves were determined by the multiple-specimen technique first proposed by Landes and Begley [17]. This method consists of loading a series of identical specimens to various subcritical displacements, producing different amounts of crack extension, Δa. The value of J for each specimen was determined from the load versus displacement curve by the approximate equation proposed by Rice et al. [18]:

$$J = 2(U/B)(W - a) \tag{6}$$

which is valid only for a span-to-width ratio (S/W) equal to 4 and a crack-to-width ratio (a/W) between 0.4 and 0.7 [19]. The fracture energy, U, is the area under the load deflexion curve and B is the specimen thickness. J–R curves were constructed by plotting values of J as a function of Δa.

3. Experimental

3.1. Sample preparation

3.1.1. Small scale samples

Test specimens were extracted from two different commercial polyethylene extruded pipes: a carbon black filled medium density polyethylene pipe and a natural medium density polyethylene pipe. The first pipe and its material will be referred to as P1 and PE1 respectively and the second pipe and its material as P2 and PE2 respectively. Fracture specimens were obtained from pipe sections as explained below and then machined to reach final shape and dimensions.

Because the mechanical behavior of extruded plastic pipes is not only governed by its material characteristics and pipe dimensions but also by material morphology and orientation derived from processing [20], fracture characterization in different pipe directions was conducted on specimens with different geometries.

For longitudinal–transversal fracture behavior evaluation of PE1 an arc-shaped geometry (thickness, $B = 10$ mm) obtained from transversal pipe section was used. On the other hand, for PE2 traditional SE(B) samples axially cut out from the pipes were used in order to determine circumferential–radial fracture properties.

Dumb-bell specimens for uniaxial tensile tests were also axially cut out from the pipes. The final thickness was 5 mm, gage length was 50 mm and the width was 13 mm.

Fracture experiments were conducted on the specimens in three-point bending. Thickness-to-depth ratio (B/W) and span-to-depth ratio (S/W) were always kept equal to 1 and 4 respectively. Sharp notches were introduced by sliding a sharp scalpel to a depth corresponding to crack-to-depth ratios (a/W) of 0.3 and 0.5.

Pressurized pipes in service experience a high degree of constraint from the surrounding material [21]. In order to simulate this situation, usually not found in small scale laboratory samples, fracture specimens were side-grooved after sharp notching reducing the thickness by 20%. The angle of the side grooves was 45°.

3.1.2. Full scale samples

On the other hand, 700 mm long and 125 mm outer diameter P1 pipes with axial internal cracks were machined. Wall thickness was 10 mm. Two different crack depths were used: 2.58 and 5.15 mm while crack length was kept equal to 500 mm. An un-notched pipe specimen was also used to obtain a blank test.

In order to machine straight axial notches, a specially designed device was used (Fig. 1). The device consisted on a rectangular base of 1100 mm long and 220 mm wide, where pipes were fixed. At the ends of

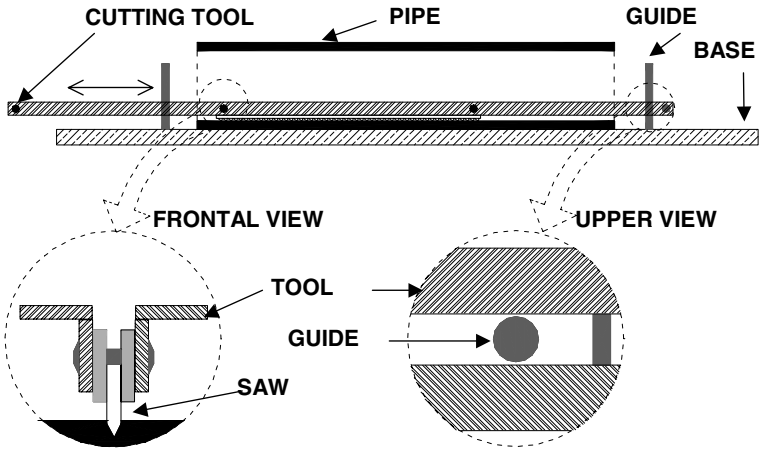

Fig. 1. Sketch of the device for machining axial notches in P1 pipes.

the base, two 10 mm diameter threaded bars were normally screwed. These bars served as guides for the cutting tool (Fig. 1) allowing a longitudinal movement. The cutting tool acted in the bore of the pipe machining notches of different depths. A commercial 300 mm long saw was used as a cutting tool. It was specially designed so that its teeth presented a single sharp prism shaped edge line. In this way, "V" notches in the deepest part of the notch were produced by avoiding lateral material laceration due to alternating deviations of the teeth.

Circumferentially cracked P2 pipes 150 mm long and 125 mm of outer diameter were also machined. Wall thickness was kept equal to 10 mm. Different crack lengths were used: 3, 6, 7 and 7.5 mm. Both circumferential internal and external notches were machined.

3.2. Mechanical testing

3.2.1. J–R curve determination

Fracture testing was carried out at 2 mm/min cross-head speed and room temperature in an Instron 4467 dynamometer.

Load–displacement traces were corrected for indentation using the test configuration recommended by the ESIS Protocol [22]. Due to the large ductility displayed by both polyethylenes, large degrees of crack tip blunting were observed, and hence large specimen displacements were allowed in order to try to measure the actual crack advance. So that J was determined from the indentation corrected area under the load–displacement curve. The materials displayed a high degree of blunting consistent with their high ductility. A relatively short a/W ratio (0.3) was also used in order to try to obtain J–R curve points within the stable propagation zone outside the blunting zone.

Circumferential–radial and longitudinal–radial J-resistance curves for medium density polyethylene were determined by the multiple-specimen technique consisting on loading a series of identical specimens to different subcritical displacements and then unloading. Then the samples were completely fractured in a Charpy pendulum at room temperature after they had been immersed in liquid nitrogen for a few minutes and the ductile tearing zone, Δa determined postmortem from the surface, using an optical microscope.

Uniaxial tensile experiments were conducted using an Instron 4467 dynamometer at 2 mm/min. The strain was continuously recorded during the test, by means of a clip/gauge extensometer having a 50 mm gauge length.

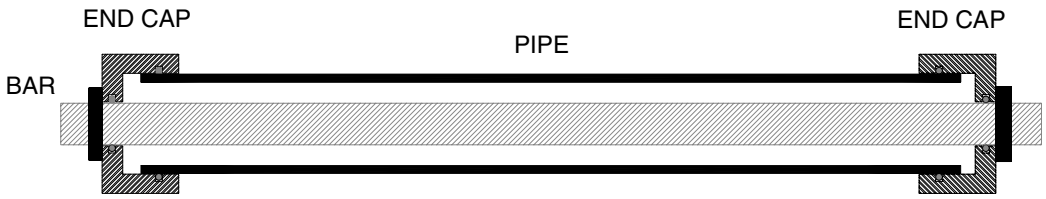

Fig. 2. Sketch of pipe section end caps and tie bar.

3.2.2. Full scale tests

Full scale burst tests of P1 pipes were carried out in the CINI laboratories, SIDERCA, Campana. Before testing, the ends of each pipe were sealed using specially designed floating end caps connected by a central coaxial tie bar. The end caps were sealed to the outside surface of the pipe and to the tie bar using O-rings type sealings (Fig. 2). After fixing the end caps, the pipe was filled with water through one of them, while the other allowed air to be expelled. Finally, the internal pressure was elevated in a controlled way until collapse had occurred. Applied pressure was continuously monitored during the tests.

Uniaxial tensile tests were conducted on full scale circumferentially flawed P2 pipes with both internal and external cracks at a cross-head speed of 2 mm/min in the Instron dynamometer. Specially designed bridle type clamping fixtures were used. Load–displacement records were obtained from these experiments.

4. Results and discussion

As explained in Section 2 the EPRI Handbook calculations require the parameters of a power-law stress–strain approximation like Ramberg–Osgood's law, widely adopted in the description of stress–strain behavior of metals [23].

The following uniaxial stress–strain relationship was considered:

$$\frac{\varepsilon}{\varepsilon_0} = \frac{\sigma}{\sigma_0} + \alpha\left(\frac{\sigma}{\sigma_0}\right)^n \tag{7}$$

where α, n and σ_0 are the power-law fitting parameters. σ_0 was determined from the maximum in the true stress–strain curve accurately obtained for strains values up to 10% and was also taken as the yield stress. The parameter ε_0 was calculated as

$$\varepsilon_0 = \frac{\sigma_0}{E} \tag{8}$$

where Young's modulus (E) was determined from the initial slope of the true stress–deformation curve.

By applying the proposed fitting (Eq. (7)), Ramberg–Osgood's parameters were found to be $\alpha = 4.9$ and $n = 3$ for PE1 polyethylene, and $\alpha = 2.1$ and $n = 2.6$ for PE2 polyethylene. The values of yield stress and Young's modulus were $\sigma_0 = 20$ MPa and $E = 948$ MPa for PE1 polyethylene and $\sigma_0 = 18.4$ MPa and $E = 839$ MPa for PE2 polyethylene.

Fig. 3a and b shows typical micrographs of the fracture surfaces of pendulum-broken samples of both polyethylenes after a significant crack extension had apparently occurred.

Fig. 4a and b shows J–R curves for both polyethylenes. The high scatter exhibited by experimental data can be attributed to the high degree of distortion displayed by the samples due to the large values of displacement used. A simple power-law J–Δa relationship ($J = X\Delta a^Y$, where X and Y are constants) was used for fitting experimental data by following the ESIS Protocol recommendations [22].

Fig. 5 shows the crack driving force diagram constructed from specific EPRI/GE equations (see Appendix A) for an internally pressurized cylinder with an axial internal crack. The J-resistance curves for

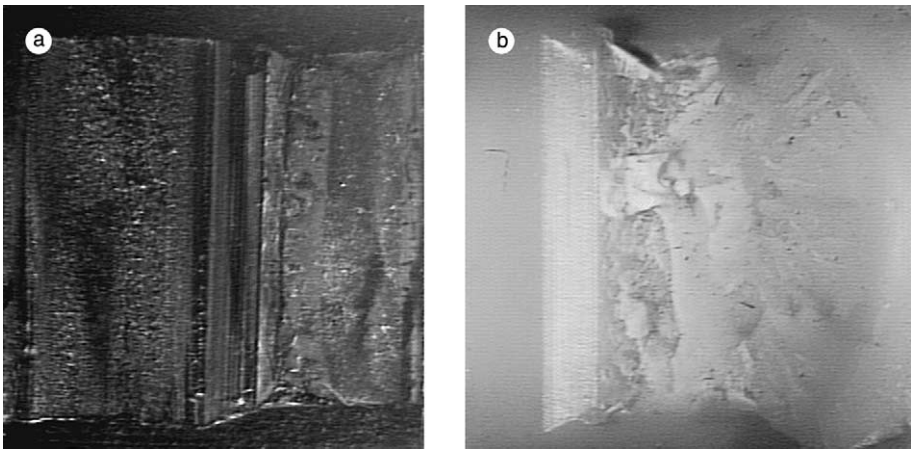

Fig. 3. Photograph of fracture surfaces of samples immersed in liquid nitrogen prior to complete fracture: (a) PE1 polyethylene, (b) PE2 polyethylene (The crack extended from the left to the right.).

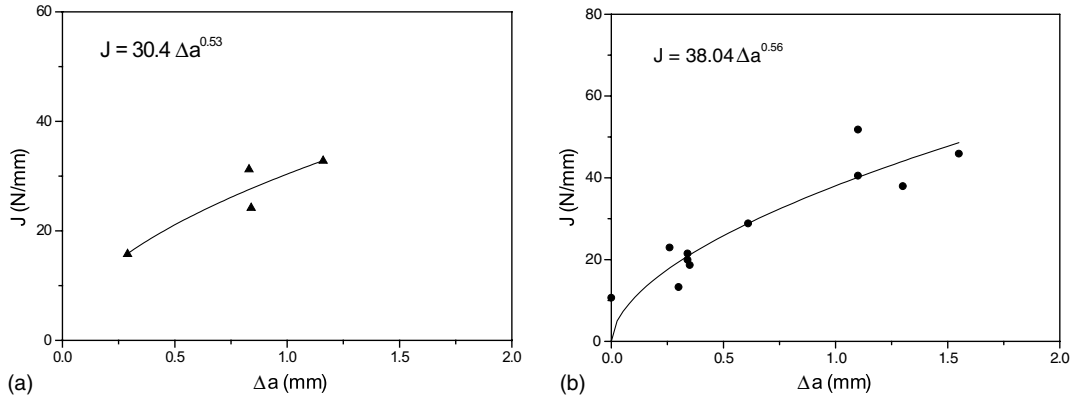

Fig. 4. *J–R* curves for both polyethylenes used in this study superimposed to the power-law fitting of experimental data: (a) PE1 polyethylene, (b) PE2 polyethylene.

$a_o = 2.58$ and 5.15 mm are superimposed to the diagram. The instability points predicted from the tangency between the *J–R* curves and the driving force diagram led to critical pressure values in apparent agreement with experimental burst pressures obtained from hydraulic tests. In Fig. 6, experimental and predicted pressure values from limit load analysis and the EPRI procedure are plotted as a function of initial crack length. Both predictions agree with experimental data.

The fracture appearance of P1 pipe in a full scale burst test showed that the pipes failed by first yielding at the reduced net cross-section along the axial notch, then rupturing circumferentially. Hence, the failure of these pipes appears to be governed by plastic collapse rather than by an actual fracture propagation phenomenon.

Fig. 7a and b shows tensile load–displacement records for P2 flawed pipes with circumferential external and internal cracks respectively. Critical loads were obtained from these records.

Fig. 8a and b shows the crack driving force diagrams for circumferentially externally and internally cracked cylinders in tension respectively. The material *J*-resistance curves for the initial crack lengths used

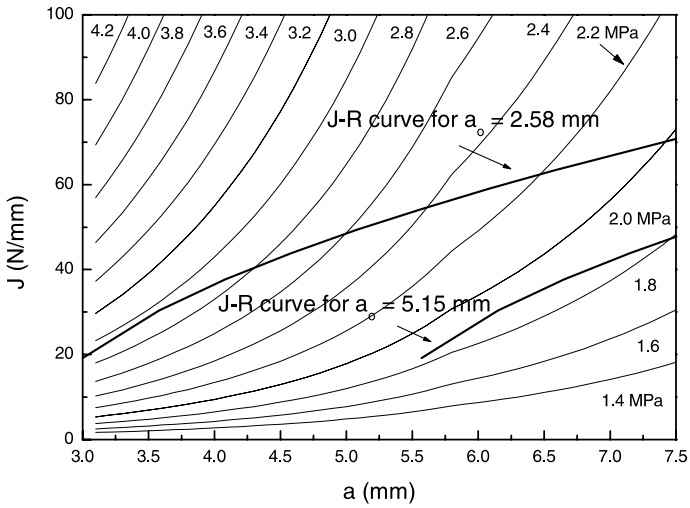

Fig. 5. Driving force diagram superimposed to material J–R curve for an internally pressurized polyethylene pipe with an internal axial crack.

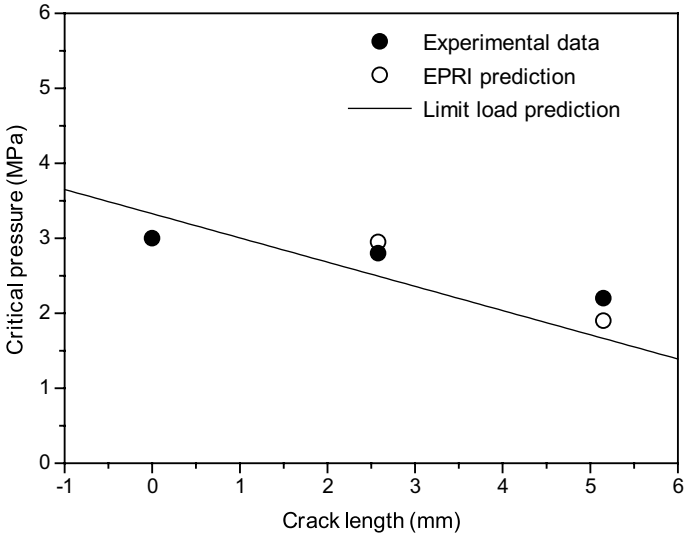

Fig. 6. Actual critical pressure values versus crack length for P1 pipes superimposed to predicted values obtained from limit load analysis and EPRI procedure.

in full scale tests are superimposed to these diagrams. The instability conditions were identified from the tangency between the resistance curves and the J versus crack length curves with load held constant.

In Fig. 9 experimental data of critical loads are compared to predicted values obtained from limit load analysis and EPRI procedure. For circumferentially internally cracked pipes, the predicted instability loads from the EPRI scheme resulted higher than critical loads obtained from uniaxial tensile tests directly conducted on flawed pipes whereas limit load predictions accurately fit actual critical loads. On the other hand, for the circumferentially externally cracked pipes both predictions reasonably agree with experimental data.

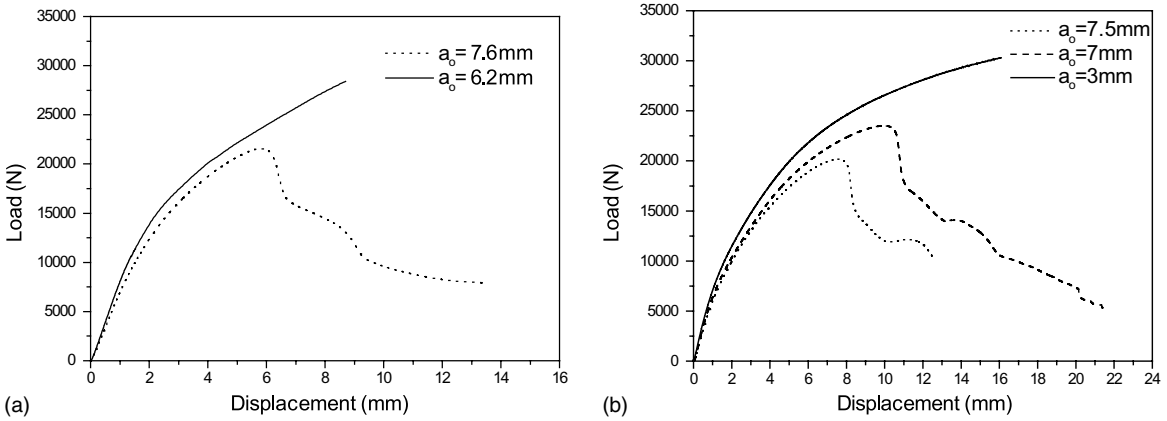

Fig. 7. Load–displacement records for P2 pipes under remote tension with circumferential cracks with different initial notch lengths: (a) external cracks, (b) internal cracks.

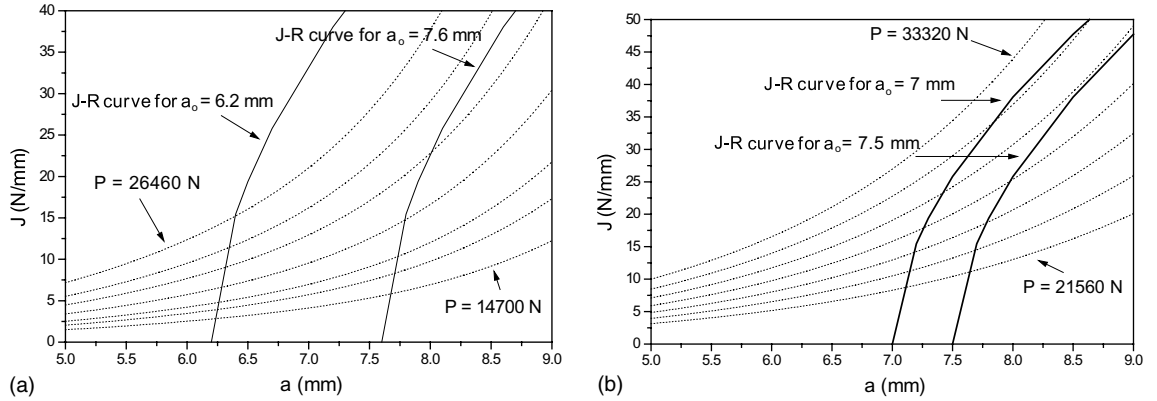

Fig. 8. Driving force diagram superimposed to material J–R curve for a cylinder with an circumferential crack under remote tension: (a) external cracks, (b) internal cracks.

In the light of the results found for internally cracked P2 pipes and due to the problems related to crack length measurements reported for these materials [8], additional tests were conducted to determine if the measured crack extensions were due to actual crack growth or due to blunting. Different methods were used to determine the increase in crack length, Δa. In the first one, apparent crack extension was evidenced by painting it with a penetrating ink before unloading. The second method was to measure the amount of crack extension from side views of polished samples.

Fig. 10 is an optical micrograph of the fracture surface of PE2 samples by using the first method for evidencing crack advance. The distinctive zone observed ahead of the crack tip can be identified as the crack tip craze zone which was separated during the fracture of the sample in the pendulum. It is well established that the fracture growth process in polyethylenes consists of the failure of the crazed material developed at the crack tip [24].

Fig. 11 is an optical micrograph of side view of a polished sample of PE2 polyethylene. Clearly only stretching with some crazes is observed in this figure without any evidence of subcritical crack growth.

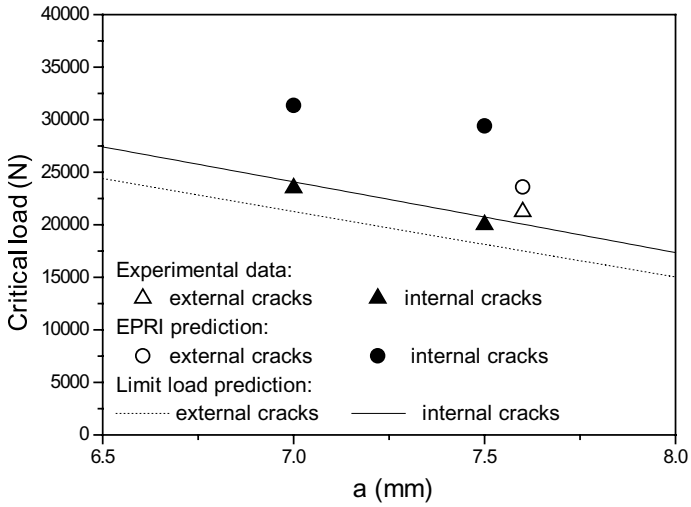

Fig. 9. Actual critical load values versus crack length for P2 pipes superimposed to predicted values obtained from limit load analysis and EPRI procedure.

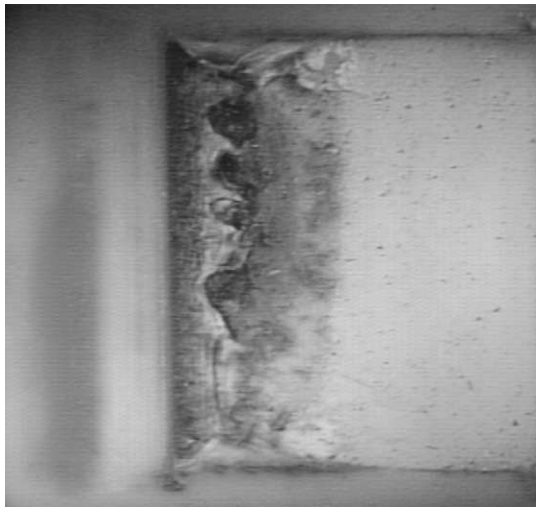

Fig. 10. Photograph of the fracture surface of a PE2 polyethylene sample painted prior to complete fracture (The crack extended from the left to the right.).

Fig. 12 shows a macrophotograph of the side view of a polished sample of PE1 polyethylene. As in the case of the PE2 polyethylene sample, in spite of the large displacements developed during the tests only stretching with no signs of stable crack extension could be observed for this sample.

Fig. 13a and b shows the J–R curves of Fig. 4 by using a linear regression of experimental data of J versus Δa instead of the power-law fit. The corresponding theoretical blunting lines which account for the apparent increase in crack length due to crack tip blunting prior to material separation are also included in these plots. They were obtained from the yield strength of the materials by assuming a smooth blunting with a semicircular profile as $J = 2\sigma_0\Delta a$ [8]. It should be noted that despite the scatter of the data, experimental points of both polyethylenes reasonably agree with their corresponding theoretical blunting

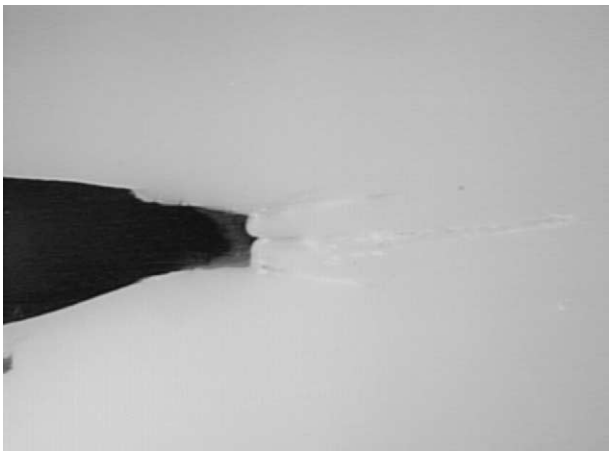

Fig. 11. Optical microphotograph of the side view of a polished sample of PE2 polyethylene (The cracks extended from the left to the right.).

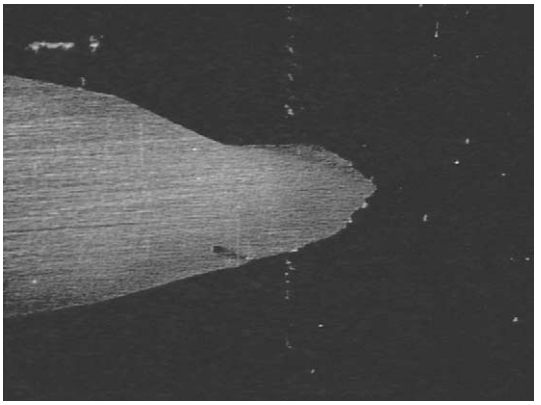

Fig. 12. Optical microphotograph of the side view of a polished sample of PE1 polyethylene (The cracks extended from the left to the right.).

lines. This reinforces the notion that no crack extension has occurred in these experiments and the apparent increase in crack length was only due to crack tip blunting. Similar results were reported in literature for medium density polyethylene [25].

Furthermore, all the techniques used to determine crack lengths led to data points that can be fitted by a single linear regression which is also very close to the theoretical blunting line (Fig. 13).

The agreement between experimental values and predicted values from limit load analysis obtained for the materials and geometries analyzed as well as the results of fracture tests indicate that fully plastic regime exists. In this regime, single-parameter fracture mechanics would only be valid provided the specimen maintains a relatively high level of triaxiality [26]. Otherwise critical fracture toughness values would exhibit a size and geometry dependence and the problem would be reduced to a limit load solution, where the main effect of the crack would be to reduce the net cross-section of the structure [14].

Our results can be explained in terms of the large craze zone that develops ahead of a crack tip in medium density polyethylene. It has been reported in literature for tough grades of polyethylenes [24,27] that this

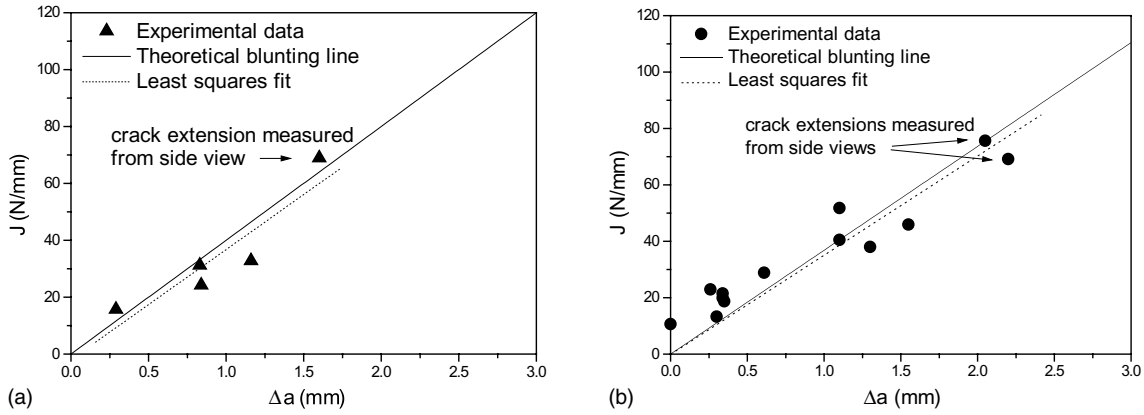

Fig. 13. *J–R* curves for both polyethylenes superimposed to the theoretical blunting lines and the least squares linear regression of experimental data: (a) PE1 polyethylene, (b) PE2 polyethylene.

zone tends to eliminate the stress singularity at the crack tip and hence to invalidate the use of a single parameter fracture analysis.

5. Conclusions

Through this paper the predictive capability of the limit load and the EPRI analyses for polymers was studied with two different defect structures, i.e., an axially flawed polyethylene pipe under internal pressure and a circumferentially cracked polyethylene pipe subjected to remote tension by comparing predicted instability points with actual values obtained from full scale tests.

For the axially cracked pipes under internal pressure, both the predicted critical pressure values from limit load analysis and EPRI scheme agree with actual burst pressures determined from hydraulic full scale tests. However, experimental observations of failed structures indicated that plastic collapse had occurred. Hence, that failure is governed by the flow properties of the material rather than its fracture toughness [14].

For the circumferentially externally cracked pipes subjected to remote tension, both the EPRI and limit load predictions reasonably agree with experimental data. On the other hand, for the circumferentially internally cracked polyethylene pipes, the predicted critical loads from the EPRI procedure overestimates measured values at failure whereas limit load predictions based on the material yield stress and net cross-section of the structures accurately fit them. The inherent assumption contained in the EPRI scheme that computed driving force parameter uniquely characterizes crack tip conditions breaks down under large scale plasticity [26,28,29].

Finally, some care should be taken to apply the EPRI procedure originally developed to failure assessment of metal structures to predict instability points in the case of ductile polymers like tough grades of polyethylenes which exhibit extensive plasticity.

Appendix A

EPRI elastic–plastic estimation formulae are

$$J = f_1(a_e; R_i/R_o)\frac{Q^2}{E'} + \alpha\varepsilon_0\sigma_0 c(a/b)h_1(a/b, n; R_i/R_o)(Q/Q_0)^{n+1} \tag{A.1}$$

Q is the pressure or load, Q_0 is the limit pressure or load in the perfectly plastic case corresponding to $n = \infty$ and a_e is the effective crack length in plane strain.

$$a_e = a + \phi r_y \tag{A.2}$$

$$r_y = \frac{1}{6\pi}\left[\frac{n-1}{n+1}\right]\left(\frac{K_I}{\sigma_0}\right)^2 \tag{A.3}$$

$$\phi = \frac{1}{1+\left(\frac{Q}{Q_0}\right)^2} \tag{A.4}$$

For an internally pressurized cylinder with an internal axial crack [16]:

$$K_I = \frac{2pR_o^2\sqrt{\pi a}}{R_o^2 - R_o^2}F(a/b, R_i/R_o) \tag{A.5}$$

$$Q_0 = \tfrac{2}{\sqrt{3}}c\sigma_0/R_c \tag{A.6}$$

where $R_c = R_i + a$ is the radial distance from the centerline to the crack tip.

$$f_1(a/b, R_i/R_o) = 4\pi a\left[\frac{R_o^2}{R_o^2 - R_i^2}\right]^2 F^2(a/b, R_i/R_o) \tag{A.7}$$

F_1 and h_1 are the functions tabulated in Ref. [30].

For a cylinder with a circumferential crack under remote tension [16]:

$$K_I = \sigma^\infty\sqrt{\pi a}F(a/b, R_i/R_o) \tag{A.8}$$

where σ^∞ is the uniform tensile stress field at the cylinder ends.

$$Q_0 = \tfrac{2}{\sqrt{3}}\sigma_0\pi(R_o^2 - R_c^2) \tag{A.9}$$

with $R_c = R_i + a$ for an internal crack and,

$$Q_0 = \tfrac{2}{\sqrt{3}}\sigma_0\pi(R_c^2 - R_i^2) \tag{A.10}$$

with $R_c = R_o - a$ for an external crack.

$$f_1(a/b, R_i/R_o) = \frac{aF_1^2(a/b, R_i/R_o)}{\pi(R_o^2 - R_i^2)^2} \tag{A.11}$$

F_1 and h_1 are the functions tabulated in Ref. [31].

References

[1] Lu X, Zhou Z, Brown N. The anisotropy of slow crack growth in polyethylene pipes. Polym Engng Sci 1994;34:109–15.
[2] Lu X, Brown N, Bassani J. The correlation of slow crack growth in linear polyethylene by the J-integral. Polymer 1989;30:2215–21.
[3] Wheel MA, Leevers PS. High speed double torsion tests on tough polymers. II: nonlinear elastic dynamic analysis. Int J Fract 1993;61:349–59.
[4] Greig JM, Leevers PS, Yayla P. Rapid crack propagation in pressurized plastic pipe. I. Full-scale and small-scale RCP testing. Engng Fract Mech 1992;42:663.
[5] Nishimura H, Nakashiba A, Nakakura M, Sasai K. Fatigue behavior of medium-density polyethylene pipes for gas distribution. Polym Engng Sci 1993;33:895–900.

[6] Frassine R, Rink M, Pavan A. Discontinuous creep crack growth in polyethylene. Plastic, Rubber Compos Process Appl 1996;25:1–5.
[7] Han L-H, Deng Y-C, Liu C-D. The determination of J_{IC} for polyethylene pipe using non-standard arc-shaped specimen. Int J Press Vess Piping 1999;76:647–51.
[8] Chung WN, Williams JG. In: Determination of J_{IC} for polymer using the single specimen method, elastic–plastic fracture test methods: the user's experience. ASTM STP 1114. 1991. p. 320.
[9] Yayla P, Leevers PS. Rapid crack propagation in pressurized plastic pipe. II. Critical pressures for polyethylene pipe. Engng Fract Mech 1992;42:675.
[10] Ritchie SJK, Davis P, Leevers PS. Brittle–tough transition of rapid crack propagation in polyethylene. Polymer 1998;39(25):6657–63.
[11] Greenshields CJ, Leevers PS. Correlation between full scale and small scale steady state (S4) tests for rapid crack propagation in plastic gas pipe. Plastic, Rubber Compos 1999;28(1):20–5.
[12] Landes JD, Brown KH, Herrera R. In: Determining failure load: ductile fracture methodology versus limit load. ASTM STP 1131. 1992. p. 158–77.
[13] Kumar V, German MD, Shih CF. An engineering approach for elastic–plastic fracture analysis. EPRI Report NP-1931, 1981.
[14] Anderson TL. Fracture mechanics: fundamentals and applications. CRC Press; 1995. p. 493.
[15] Beer FP, Johnston ER. Mechanics of materials. McGraw-Hill Co; 1981.
[16] Kumar V, German MD, Shih CF. An engineering approach for elastic–plastic fracture analysis. EPRI Report NP-1931, Sections 4.2 and 4.3, 1981.
[17] Landes JD, Begley JR. In: Tests results from J-integral studies an attempt to establish a J_{IC} testing procedure. ASTM STP 560. 1974. p. 170–86.
[18] Rice JR, Paris PC, Merkle JC. In: Some further results on J-integral analysis and estimates. ASTM STP 536. 1973. p. 231–45.
[19] Huang DD. In: Joyce JA, editor. The Application of the multispecimen J-integral technique to toughened polymers. ASTM STP 1114. 1991. p. 290–305.
[20] Kanninen MF, O'Donoghue PE, Popelar CH, Kenner VH. Engng Fract Mech 1990;36:903–18.
[21] Frassine R, Rink M, Pavan A. Size effects in the fracture of a pipe-grade high density polyethylene. Fatigue Fract Engng Mater Struct 1997;20(8):1217–25.
[22] A testing protocol for conducting J-crack growth resistance curve tests on plastics. ESIS-TC4 Polymers and Composites, Cambridge, 1991.
[23] Miller AG, Aisnwoth RA. Consistency of numerical results for power-law hardening materials and the accuracy of the reference stress approximation. J Engng Fract Mech 1989;32:233–47.
[24] Duan D-M, Williams JG. Craze testing for tough polyethylene. J Mater Sci 1998;33:625–38.
[25] Ramsteiner F, Schuster W, Forster S. Concepts of fracture mechanics for polymers. In: Grellmann, Seidler, editors. Deformation and fracture behaviour of polymers. Berlin: Springer-Verlag; 2001. p. 27.
[26] Anderson TL. Fracture mechanics: fundamentals and applications. CRC Press; 1995. p. 155.
[27] Pandya KC, Williams JG. Measurement of cohesive zone parameters in tough polyethylene. Polym Engng Sci 2000;40(8):1765–76.
[28] Anderson TL. Fracture mechanics: fundamentals and applications. CRC Press; 1995. p. 509.
[29] Anderson TL. Fracture mechanics: fundamentals and applications. CRC Press; 1995. p. 508.
[30] Kumar V, German MD, Shih CF. An engineering approach for elastic–plastic fracture analysis. EPRI Report NP-1931, Tables 4.1 and 4.2, 1981.
[31] Kumar V, German MD, Shih CF. An engineering approach for elastic–plastic fracture analysis. EPRI Report NP-1931, Tables 4.5 and 4.6, 1981.